THE COMPACT CIRCUMSTELLAR MATERIAL AROUND OH 231.8+4.2[1]

M. Matsuura,[2,3,4] O. Chesneau,[5] A. A. Zijlstra,[2] W. Jaffe,[6] L. B. F. M. Waters,[7,8] J. A. Yates,[9]
E. Lagadec,[2] T. Gledhill,[10] S. Etoka,[2] and A. M. S. Richards[11]

ABSTRACT

We have observed the bipolar post–asymptotic giant branch candidate OH 231.8+4.2, using the mid-infrared interferometer MIDI and the infrared camera with the adaptive optics system NACO on the Very Large Telescope. An unresolved core (<200 mas in FWHM) is found at the center of OH 231.8+4.2 in the 3.8 μm image. This compact source is resolved with the interferometer. We used two 8 m telescopes with four different baselines, which cover projected baseline lengths from 62 to 47 m, and projected position angles from 112° to 131° that are almost perpendicular to the bipolar outflow. Fringes from 8 to 9 μm and from 12 to 13.5 μm were clearly detected, while strong silicate self-absorption allows only marginal detection of visibilities between 9 and 12 μm. The fringes from the four baselines consistently show the presence of a compact circumstellar object with an inner radius of 30–40 mas, which is equivalent to 40–50 AU at 1.3 kpc. This clearly shows that the mid-infrared compact source is not the central star (3 AU) but circumstellar material. The measured size of the circumstellar material is consistent with the size of such disks calculated by hydrodynamic models, implying that the circumstellar material may be in a disk configuration.

Subject headings: dust, extinction — infrared: stars — ISM: jets and outflows — stars: AGB and post-AGB —
stars: mass loss

1. INTRODUCTION

Low- and medium-mass stars (~1–8 $M_\odot$ on the main sequence) experience an intense mass-loss phase during the asymptotic giant branch (AGB) phase. Typically, the AGB wind is spherically symmetric. However, during the following evolutionary stages, that is, the post-AGB phase and the planetary nebula (PN) phase, a large fraction of stars display asymmetric shapes, such as elliptical and bipolar, in their circumstellar envelopes. One hypothesis about the formation of the bipolar shape invokes a binary disk scenario (Balick & Frank 2002; Van Winckel 2003). Part of the material lost during the intense AGB mass-loss wind is trapped in the binary system, and a circumbinary disk is formed in the plane of the binary orbit. The disk restricts the direction of the low-density but high-velocity post-AGB and PN wind in the equatorial plane and focuses the wind toward two poles. The size of the binary disk will be small (less than 100 AU [80 mas for our target]; Mastrodemos & Morris 1999) and so requires interferometric observations to be resolved.

[2] School of Physics and Astronomy, University of Manchester, P.O. Box 88, Manchester M60 1QD, UK.

[3] School of Mathematics and Physics, Queen's University Belfast, University Road, Belfast BT7 1NN, UK.

[4] National Astronomical Observatory of Japan, 2-21-1 Osawa, Mitaka, Tokyo 181-8588, Japan.

[5] Observatoire de la Côte d'Azur, Avenue Nicolas Copernic, F-06130 Grasse, France.

[6] Sterrewacht Leiden, Postbus 9513, NL-2300 RA Leiden, Netherlands.

[7] Sterrenkundig Instituut Anton Pannekoek, Universiteit van Amsterdam, Kruislaan 403, NL-1098 SJ Amsterdam, Netherlands.

[8] Instituut voor Sterrenkunde, Katholieke Universiteit Leuven, Celestijnenlaan 200B, B-3001 Heverlee, Belgium.

[9] Department of Physics and Astronomy, University College London, Gower Street, London WC1E 6BT, UK.

[10] Centre for Astrophysics Research, Science and Technology Research Institute, University of Hertfordshire, College Lane, Hatfield AL10 9AB, UK.

[11] Jodrell Bank Observatory, University of Manchester, Jodrell Bank, Lower Withington, Macclesfield SK11 9DL, UK.

OH 231.8+4.2 (IRAS 07399−1435; R.A. = 07^{h}42^{m}16^s.83, decl. = −14°42′52″.1; J2000), hereafter OH 231, is a well-studied post-AGB candidate. TiO bands are detected from the central region, suggesting that the central star exhibits an M9 spectral type (Cohen 1981). Sánchez Contreras et al. (2004) claimed the presence of a spectroscopic binary from optical spectra, because in addition to TiO and VO bands from the M-type star, Balmer lines and continuum excess are detected. OH 231 is probably located in the open cluster M46 (Jura & Morris 1985), and thus the distance is relatively well determined (1.3 kpc).

The outflow is strongly bipolar, and bubbles and shocked regions are found in the outflow (see, e.g., Bujarrabal et al. 2002). *L*-, *N*-, and *Q*-band seeing-limited images show an unresolved core at the center of this object (Kastner et al. 1992; Jura et al. 2002). The infrared color of this compact source is extremely red, and it is believed to be a dusty disk (Jura et al. 2002). The velocity structure of SiO masers also suggests the presence of a rotating disk around this compact source (Sánchez Contreras et al. 2002). The OH masers appear to be associated with an expanding torus (Zijlstra et al. 2001).

In this Letter, we present both high-resolution infrared images and mid-IR interferometric visibilities of the central compact source, so as to resolve the compact source at the center and determine if this source is a disk.

2. OBSERVATIONS AND ANALYSIS

OH 231 was observed with the mid-IR interferometric instrument (MIDI; Leinert et al. 2003) on the Very Large Telescope (VLT) on 2005 March 2 (UT), using unit telescopes Melipal and Yepun. The observation log is summarized in Table 1. From these observing runs, we also obtained acquisition images (single-dish) with the adaptive optics (AO) system, spectrophotometric data, and visibilities (correlated fluxes) for each baseline.

The data reduction software packages MIA and EWS (Jaffe 2004; Chesneau et al. 2005) were used to reduce the spectra and visibilities. To estimate errors in the visibility data, the MIA visibilities were extracted with three different thresholds
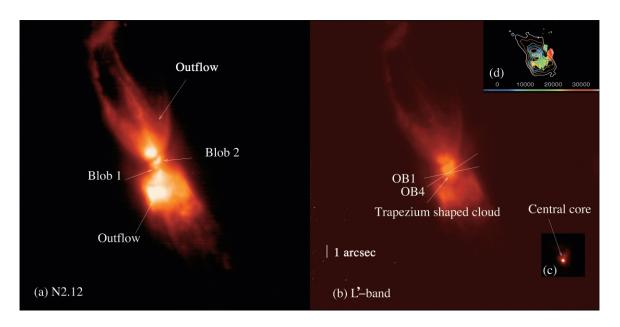
FIG. 1.—(a–c) Near-infrared adaptive optics images of OH 231. Lines in (b) show the approximate baseline position angle of OB1 and OB4 for MIDI observations. Inset (c) shows the brightest region of the L'-band image in a different color scale so as to clearly show the unresolved "central" object inside. North is up, and east is to the left. The color in inset (d) shows the OH maser velocity map, superposed on the L'-band ISAAC contour image. Note that the scale in (d) is 16 × 20 arcsec², which is different from that in (a), (b), and (c).

of noise level, and the difference in the visibilities between these thresholds are counted as errors. The difference between visibilities due to the choice of the calibration data was counted as a systematic error and added to the errors derived above. The EWS visibilities are slightly higher than the MIA ones but well within the error bars.

For spectrophotometry, we used Cohen et al.'s (1999) templates of HD 139127 (K4.5 III) for HD 50778 (K4 III) and of HD 180711 (G9 III) for HD 61935 (G9 III) and scaled the flux to *IRAS* 12 μm measurements. The spectrophotometric error bars were estimated from eight calibrated spectra that were recorded.

We observed OH 231 with the AO system and the infrared camera NACO (Rousset et al. 2003; Lenzen et al. 2003) on the VLT on 2004 March 6 (UT). The exposure time was 7.5 minutes for the NB2.12 band and 4.8 minutes (positive image only) for the L' band. Both filters measure continuum emission. The NB2.12 filter ($\lambda_c = 2.122$ μm and $\Delta\lambda = 0.022$ μm) is designed to detect the H$_2$ 1–0 S(1) line; however, spectroscopic observations using the ISAAC instrument showed no detection of this line, and the NB2.12 band measured continuum emission, probably scattered light. We used the S27 and L27 cameras (pixel scale of 27 mas). The central wavelength is 3.80 μm and the width is 0.62 μm for the L' band. The wave-front sensor

was used in visible light provided by an AO reference star ($V = 14.2$ mag) approximately 35″ from the central compact object, giving a Strehl ratio of about 30% at 2.12 μm. A neutral density filter was used for the L'-band observations, which reduced the energy by 1.5%–2%. The jittering technique was used to minimize the effect of hot pixels, and the sky background was estimated from a median of jittered frames with different positions. A chopping technique was used during the L'-band observations with a throw of 10″ to the east and the west.

MERLIN phase-referenced observations of the 1667 MHz OH maser line were obtained on 2005 April 25, using a velocity resolution of 0.7 km s^{-1}. The observations covered the velocity range $v_{LSR} = -20$ to $+80$ km s^{-1}. The angular resolution is about 0″.2. The data were reduced using AIPS. Velocity maps were obtained by calculating moment maps. The systemic velocity is about 35 km s^{-1} (Zijlstra et al. 2001).

3. DATA DESCRIPTION AND INTERPRETATION

Figure 1 shows NACO NB2.12 and L' images of OH 231. The central region is still obscured in the NB2.12 image, and the bipolar outflow is brighter. On the other hand, in the L' band the central region is brighter than the outflow. This shows

TABLE 1
OBSERVING LOG FOR MIDI

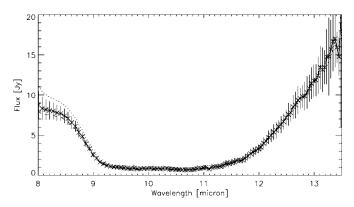| Observation | TIME (UT 2005 Mar 2) | AIR MASS | PROJECTED BASELINE | | Size[a] (mas) |
			Length (m)	P.A. (deg)	
OB1 (OH 231)	02:04–02:07	1.02	61.7	112.0	...
OB2 (OH 231)	02:53–02:55	1.06	58.9	116.2	...
OB3 (OH 231)	03:55–03:57	1.19	52.8	123.8	...
OB4 (OH 231)	04:38–04:40	1.35	47.4	131.2	...
Calibrations					
Cal. 1 (HD 50778)	02:29–02:31	1.11	56.2	117.8	3.76 ± 0.04
Cal. 2 (HD 61935)	03:12–03:14	1.12	56.0	116.4	2.21 ± 0.01
Cal. 3 (HD 61935)	04:14–04:16	1.30	48.3	123.8	...

[a] Theoretical size of the calibration stars.

FIG. 2.—Spectra of OH 231. *Bold solid line*, total spectrum using OB1–OB4 data, together with the error bars; *dotted line*, spectrum reduced from OB1 (calibrator: HD 50778); *dashed line*, spectrum reduced from OB2, OB3, and OB4 (calibrator: HD 61935). The difference below 8.5 μm is probably caused by the uncertainty of SiO band intensities in the spectra of the calibrators.

that this central region has a very red color, due to obscuration by extremely high optical depth or to its having a very low temperature, as suggested by previous infrared observations (Kastner et al. 1992; Bujarrabal et al. 2002).

In the NB2.12-band image, the central region consists of patchy clouds (blobs), which were also seen in near-IR *Hubble Space Telescope* images (Bujarrabal et al. 2002; Meakin et al. 2003). A smooth $\sim 1 \times 1$ arcsec^2 trapezium-shaped cloud with a bright central core is found in the L'-band image (Fig. 1c). This trapezium has an elongation toward the northwest. The shape resembles images at 11.7 and 17.9 μm obtained with Keck I (Jura et al. 2002).

Inside the trapezium cloud in the L'-band image, there is a bright, pointlike source. The NACO observations were unable to resolve this source, suggesting that its size is less than 0.20×0.17 arcsec^2 (FWHM). This provides a more stringent limit than Jura et al. (2002), who reported an unresolved source with dimensions of $\sim 1 \times 1$ arcsec^2 at 11 μm. Our MIDI single-dish acquisition images at 8.7 μm using the AO system (about 0″.25 resolution) also did not resolve the source.

Figure 2 shows mid-IR spectra of OH 231 obtained with MIDI. This spectrum shows the flux detected from the compact source only. There is strong silicate absorption from 9 to 11 μm; however, the flux is not completely zero, being ~ 1 Jy. The silicate absorption band is broad for this source. Gillett & Soifer (1976) and *IRAS* Low Resolution Spectrometer observations show 43 and 30 Jy at 8 μm, respectively, and Meixner et al. (1999) reported 25 Jy at 8.8 μm, while our flux is 9 Jy at 8 μm. Our spectra are from the small core region (about 0.5 × 0.3 arcsec^2), whereas other measurements for this object are from more extended regions, up to 2×5 arcsec^2 (Jura et al. 2002). Variability in the mid-IR is known for this object (Jura et al. 2002) but is not the major reason for the flux discrepancy.

We detected fringes with MIDI from "the red and pointlike source" found in the near- and mid-IR images. Figure 3 shows the correlated flux obtained with MIDI. Correlated flux is clearly recorded below 9 μm and above 11 μm, but there is only a marginal detection (~ 0.1 mJy) at 9–11 μm. At the wavelength covering the silicate absorption the visibilities are small, either because the flux level from this infrared source is too low or because the source is extended at this wavelength range.

The visibility data are interpreted in the frame of a smooth Gaussian profile, as described by Leinert et al. (2004). The assumption of a Gaussian profile is appropriate if the object is optically thin or is mildly optically thick. Figure 4 shows radii
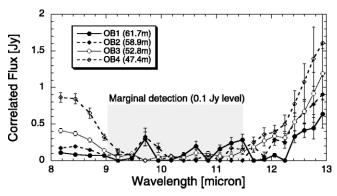

FIG. 3.—Correlated flux of the mid-infrared "core."

for the Gaussian (given in terms of the half-width at half-maximum, or HWHM) required to reproduce the observed visibilities at each wavelength. We clearly see that the structure is resolved on a 30–45 mas scale. At the distance of 1.3 kpc (Jura et al. 2002), the radii are about 40–50 AU, as displayed on the right axis in Figure 4.

The position angles of these four baselines vary by only 15°. The observed differences in the correlated flux between the four baselines seen in Figure 3 are mainly due to the baseline length, rather than any asymmetry in the object. This is confirmed by the absence of a significant dependence of the Gaussian radii on the baseline lengths at each wavelength point (Fig. 4). These correlated fluxes are therefore resolving structures on scales of 60–80 mas in FWHM.

Figure 1d presents the velocity distribution of the 1667 MHz maser emission in meters per second detected by MERLIN. The OH maser data are overplotted on the ISAAC L'-band image. It shows a clear velocity gradient along the torus-like maser distribution. Only blueshifted velocities were detected by MERLIN.

4. DISCUSSION

Our L'-band image and N-band acquisition image using the AO system find an unresolved compact object in the center of OH 231 with dimension less than 200 mas. This object has a red color and consists of circumstellar material. This circumstellar material is responsible for the fringes detected by mid-IR interferometry.

There are other emission mechanisms that can cause correlated flux in the mid-IR, such as (1) the central star and (2) the central star plus binary companion(s), but we can exclude these possibilities. First, the correlated flux of a single star with a radius of 3 AU (Sánchez Contreras et al. 2002) at 1.3 kpc (2.3 mas) is almost 100% of the total flux (i.e., unresolved)
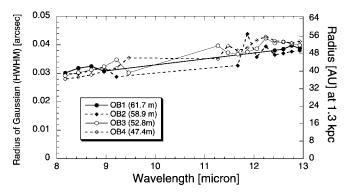

FIG. 4.—Radius (half the FWHM of the Gaussian) to reproduce the visibilities.

with current baseline lengths. The observed fringes indicate a much larger source size. Using the parameters of the central star from Jura et al. (2002; $T_{eff} = 2500$ K, radius 4.6×10^{13} cm), the flux of the central star is ~6 Jy at 10 μm, and thus the correlated flux should also be ~6 Jy on any baseline. The measured values are inconsistent with the expected correlated flux; the flux drops to 0.1–0.2 Jy for the longest baseline. Thus, the measured visibilities are not from the central star. Second, silicate absorption is detected in the correlated flux, which shows the circumstellar origin of the mid-IR compact source. Although the presence of a binary companion has been suggested by Sánchez Contreras et al. (2004), it is unlikely that we measured the orbit of the binary companion around the central star or the radius of the binary companion. A sharp angular dependence of visibilities would be expected in the orbit case, which is not detected (Fig. 4). The possibility of the binary companion's radius is ruled out because the flux would be at the 1 mJy level at 1.3 kpc if the companion was an A0 V star (Sánchez Contreras et al. 2004). Therefore, the MIDI visibilities are due to dusty circumstellar material. The absence of stellar emission in the correlated flux suggests this material is still optically thick at 10 μm.

Jura et al. (2002) analyzed the spectral energy distribution of this object and argued that the mid-IR unresolved source is a disk. Sánchez Contreras et al. (2002) measured the velocity distribution of SiO maser lines. The SiO masers show the presence of a rotating disk, within 4 mas of the star. Zijlstra et al. (2001) find that OH velocity structure could be viewed as an expanding torus, with an additional component from a bipolar, ballistic outflow.

Our NACO images also suggest the presence of a disk or torus. The central region in the L' band shows a trapezium shape: this may be interpreted as a flared outflow from a torus or a disk. The trapezium shape is also seen in the NB2.12 image. The small blobs seen in the trapezium cloud of the NB2.12 image are probably due to nonuniform extinction within the flared disk, or an illusion caused by scattered light. The north part of the "trapezium region" is brighter than other regions in NB2.12, possibly because the disk is slightly inclined, with the northern part nearer to Earth.

The obtained size of the dense circumstellar material is at least 40–50 AU. The optical depth from our preliminary analysis using DUSTY (Ivezić & Elitzur 1997) suggests $\tau_{8\,\mu m} = 1.6$ and $\tau_{13\,\mu m} = 2.7$, showing that the actual inner radius is smaller than the values that we measured. Nevertheless, if the density distribution is $\rho = \rho_0 (r/r_0)^{-\alpha}$, where $\alpha = 1$–2, the optical depth increases dramatically for closer inner radii and the measured size need not be that different from the actual inner radius of the dusty shell or torus. The hydrodynamic model of Mastrodemos & Morris (1999) shows that an accretion disk with a radius of 40–50 AU can be formed in a binary disk. The coincidence of the radii from theory and the observations implies that the circumstellar material is shaped as a disk or torus in this object.

On the other hand, Jura et al. (2002) assumed a binary companion with an orbit of 3–5 AU for OH 231, and the inner radius of the disk might be ~1.7 larger than the companion orbit, which should be 5–9 AU. Our measured inner radius is much larger than Jura et al.'s assumption. This may be because the companion is actually farther out than expected due to the central star being larger than expected by Jura et al., or because our mid-IR measurements observe the radius at which the disk has cooled down enough to allow dust to condense out of the gas phase. An alternative solution could be that the disk is gradually expanding and losing momentum, and at the time of the formation, the disk could have been much smaller than the current size. In conclusion, we measure the angular size of the circumstellar material in OH 231 to be 40–50 AU, and this material is probably in a disk or toroidal configuration. Future MIDI observations with different baseline angles are required in order to confirm the presence of a disklike structure and to measure its inclination angle.

The OH masers are located to the south and east, within the darker lane seen in the L'-band image, and trace the waist of the trapezium, allowing for orientation effects. Only foreground (blueshifted) OH is seen: the red emission appears to be more extended and is not picked up by the MERLIN interferometer, while the blue emission consists of more compact components. The velocity field shows a clear gradient in the southern part of the maser spots, with $v_{LSR} = 20$–30 km s^{-1} on the east and west edges and the bluest component ($v_{LSR} = 10$ km s^{-1}) in the middle. It is inconsistent with an expanding torus but is consistent if we are observing the blueshifted rim of a biconical outflow tilted toward us. Thus, the dynamics of the source changes from a rotating disk in the very center, within a few stellar radii, to a conical outflow at ~1000 AU. The stellar position estimated by the SiO maser tracing an equatorial rotating torus (Sánchez Contreras et al. 2002) coincides with the central position of the blueshifted (~0–5 km s^{-1}) biconical distribution seen in OH.

All the components of the binary disk hypothesis (Balick & Frank 2002; Van Winckel 2003) may therefore be present in OH 231.8+4.2: a rotating SiO maser disk very close to the central star, compact circumstellar material at ~40–50 AU that may have a disklike distribution, and a bipolar outflow.

REFERENCES

Balick, B., & Frank, A. 2002, ARA&A, 40, 439
Bujarrabal, V., Alcolea, J., Sánchez Contreras, C., & Sahai, R. 2002, A&A, 389, 271
Chesneau, O., et al. 2005, A&A, 435, 1043
Cohen, M. 1981, PASP, 93, 288
Cohen, M., Walker, R. G., Carter, B., Hammersley, P., Kidger, M., & Noguchi, K. 1999, AJ, 117, 1864
Gillett, F. C., & Soifer, B. T. 1976, ApJ, 207, 780
Ivezić, Ž., & Elitzur, M. 1997, MNRAS, 287, 799
Jaffe, W. J. 2004, Proc. SPIE, 5491, 715
Jura, M., Chen, C., & Plavchan, P. 2002, ApJ, 574, 963
Jura, M., & Morris, M. 1985, ApJ, 292, 487
Kastner, J. H., Weintraub, D. A., Zuckerman, B., Becklin, E. E., McLean, I., & Gatley, I. 1992, ApJ, 398, 552

Leinert, C., et al. 2003, Messenger, 112, 13
———. 2004, A&A, 423, 537
Lenzen, R., et al. 2003, Proc. SPIE, 4841, 944
Mastrodemos, N., & Morris, M. 1999, ApJ, 523, 357
Meakin, C. A., Bieging, J. H., Latter, W. B., Hora, J. L., & Tielens, A. G. G. M. 2003, ApJ, 585, 482
Meixner, M., et al. 1999, ApJS, 122, 221
Rousset, G., et al. 2003, Proc. SPIE, 4839, 140
Sánchez Contreras, C., Gil de Paz, A., & Sahai, R. 2004, ApJ, 616, 519
Sánchez Contreras, C., Desmurs, J.-F., Bujarrabal, V., Alcolea, J., & Colomer, F. 2002, A&A, 385, L1
Van Winckel, H. 2003, ARA&A, 41, 391
Zijlstra, A. A., Chapman, J. M., te Lintel Hekkert, P., Likkel, L., Comeron, F., Norris, R. P., Molster, F. J., & Cohen, R. J. 2001, MNRAS, 322, 280